Chinese Journal of Catalysis 42 (2021) 2287–2295

available at www.sciencedirect.com

ScienceDirect

journal homepage: www.sciencedirect.com/journal/chinese-journal-of-catalysis

Article

Different roles of MoO_3 and Nb_2O_5 promotion in short-chain alkane combustion over Pt/ZrO_2 catalysts

Bingheng Cen, Cen Tang, Jiqing Lu, Jian Chen #, Mengfei Luo *

Key Laboratory of the Ministry of Education for Advanced Catalysis Materials, Zhejiang Key Laboratory for Reactive Chemistry on Solid Surfaces, Institute of Physical Chemistry, Zhejiang Normal University, Jinhua 321004, Zhejiang, China

ARTICLE INFO

Article history:
Received 23 December 2020
Accepted 28 January 2021
Available online 10 September 2021

Keywords:
Pt/ZrO_2 catalyst
Alkanes combustion
MoO_3 promoter
Nb_2O_5 promoter
Active site

ABSTRACT

Pt/ZrO_2 catalysts promoted with MoO_3 and Nb_2O_5 were tested for the combustion of short-chain alkanes (namely, methane, ethane, propane, and *n*-hexane). For short-chain alkane combustion, the inhibition of MoO_3 (for the methane reaction) dramatically transformed to promotion (for the ethane, propane, and *n*-hexane reactions) as the carbon chain length increased, whereas the remarkable promotion of Nb_2O_5 gradually weakened with an increase in the carbon chain length. Based on a detailed study of the oxidation reactions of methane and propane over the catalysts, the different roles of the promoters in the reactions were ascribed to differences in the acidic properties of the surface and the oxidation or reduction states of the Pt species. The MoO_3 promoter could decorate the surface of the Pt species for a $Pt\text{-}Mo/ZrO_2$ catalyst, whereas the Nb_2O_5 promoter on the support could be partially covered by Pt particles for a $Pt\text{-}Nb/ZrO_2$ catalyst. The formation of accessible $Pt\text{-}MoO_3$ interfacial sites, a high concentration of metallic Pt species, and a high surface acidity in $Pt\text{-}Mo/ZrO_2$ were responsible for the enhanced activity for catalytic propane combustion. The lack of enough accessible $Pt\text{-}Nb_2O_5$ interfacial sites but an enhanced surface acid sites in $Pt\text{-}Nb/ZrO_2$ explained the slight improvement in activity for catalytic propane combustion. However, the stabilized Pt^{n+} species in $Pt\text{-}Nb/ZrO_2$ were responsible for the much-improved activity for methane combustion, whereas the Pt^{n+} species in $Pt\text{-}Mo/ZrO_2$ could be reduced during the oxidation reaction, and the fewer exposed surface Pt species because of MoO_3 decoration accounted for the inhibited activity for methane combustion. In addition, it can be concluded that MoO_3 promotion is favorable for the activation of C–C bonds, whereas Nb_2O_5 promotion is more beneficial for the activation of C–H bonds with high energy.

1. Introduction

Because air pollution caused by the massive emission of volatile organic compounds (VOCs) is a serious threat to us, effective methods for VOC elimination have attracted much attention [1–3]. Catalytic combustion (or deep oxidation) is a promising method for VOC elimination because of its significant advantages, such as high efficiency and low energy costs [4–6]. Among the various VOCs, short-chain alkanes (such as propane) with high-energy C–H bonds are very difficult to oxidize deeply and are therefore used as representative reactants to evaluate catalytic performance [7–9]. Various non-noble metal oxides (Ce, Co, Mn, Cu, etc.) and noble catalysts (Pt, Pd, Ru, etc.) [10–17] can be used as effective catalysts. For instance, Lu *et al*.

* Corresponding author. E-mail: mengfeiluo@zjnu.cn
# Corresponding author. E-mail: jianchen@zjnu.cn
This work was supported by the National Natural Science Foundation of China (21872124, 22072137).
DOI: 10.1016/S1872-2067(20)63771-8 | http://www.sciencedirect.com/journal/chinese-journal-of-catalysis | Chin. J. Catal., Vol. 42, No. 12, December 2021

[18] reported that Co_3O_4/ZSM-5 synthesized by hydrothermal methods showed high catalytic activity and stability for propane combustion with T_{90} at only 260 °C, which could be ascribed to the good reducibility of the Co^{3+} species and fast migration of the lattice oxygen atoms of Co_3O_4. However, noble catalysts normally exhibit higher catalytic activity and thermal stability than non-noble catalysts. Zhang *et al*. [19] found that irreducible-oxide-modified Pd/$MgAl_2O_4$ catalysts exhibited very high activity and excellent stability against both hydrothermal aging and deactivation under wet conditions for methane combustion. Thus, the investigation of catalytic alkane combustion (such as that of methane and propane) mainly focuses on noble catalysts, especially Pt- and Pd-based catalysts. Pt-based catalysts commonly show high catalytic activity for longer chain alkanes such as propane, whereas Pd-based catalysts are more efficient for methane combustion at low temperatures [20,21].

Although progress has been made in the catalytic combustion of short-chain alkanes, previous works were mainly an evaluation of the activity for the combustion of only a single alkane compound as the reactant; few studies have been reported on the combustion of multiple alkanes (such as methane, ethane, and propane). The benefit of such comparative investigation is that it may clarify some relevant issues in the field. For example, the exact definition of the active sites and catalytic mechanism for different alkanes over Pt catalysts is still debatable. Metiu *et al*. [22] concluded that cationic Pt^{n+} species were important active sites for methane combustion and the increase in Pt^{n+} species on the catalyst surface was responsible for the significant enhancement of methane oxidation activity. Yet, Liu *et al*. [23] concluded that metallic Pt^0 species played key roles in propane combustion. In addition, the performance of the Pt-based catalysts could be improved by adding promoters. Liao *et al*. [24] concluded that the formation of Pt-WO_3 interfaces in the Pt-WO_3/BN catalyst obviously increased the activity for propane combustion. Similar findings were also reported with Pt-MoO_3/ZrO_2 catalysts for propane combustion [25], and Wu *et al*. [26] demonstrated that the electronic interaction of Pt-TiO_x interfaces could stabilize reactive Pt^0 sites, which resulted in outstanding activities and high stability for propane and propylene combustion over a Pt@TiO_x/TiO_2 catalyst.

The aim of this work is to investigate the roles of promoters in the catalytic combustion of different alkanes. Based on our previous works, it was found that MoO_3 and Nb_2O_5 promoters could significantly improve the activity of Pt-based catalysts for propane combustion, although the performance for the combustion of other short-chain alkanes was still unclear [21,25]. Therefore, Pt/ZrO_2 catalysts promoted with MoO_3 and Nb_2O_5 were tested for short-chain alkane (methane, ethane, propane, and *n*-hexane) combustion, and very different catalytic behaviors were observed. It was found that addition of the oxides in the catalyst resulted in changes to the structures and the oxidation or reduction states of the Pt active sites, as well as the acidic properties of the catalyst surface, which consequently exerted profound effects on the observed behaviors.

2. Experimental

2.1. Synthesis of catalysts

The ZrO_2 support was prepared according to our previous work, namely, by calcination of $ZrOCO_3$ (99%, Shanghai Diyang Chemical Co., Ltd.) at 600 °C [25].

The Mo/ZrO_2 and Nb/ZrO_2 samples were synthesized by a facile impregnation method. Typically, a certain amount of $(NH_4)_6Mo_7O_{24}{\cdot}4H_2O$ or $C_4H_4NNbO_9{\cdot}xH_2O$ (both Sinopharm Chemical Reagent Co. Ltd, China.) was dissolved in deionized water (50 mL). Then, 10 g of ZrO_2 were added to the solution with stirring. The mixture was stirred for 12 h at room temperature and dried in a water bath at 90 °C. The solid was then put into an oven with a temperature of 100 °C for 5 h and calcined at 500 °C in static air for 4 h (heating rate of 10 °C min^{-1}). The obtained sample was designated as Mo/ZrO_2 or Nb/ZrO_2, and the content of metal (Mo or Nb) was 1 wt%.

The Pt-Mo/ZrO_2 and Pt-Nb/ZrO_2 catalysts were synthesized by a co-impregnation method according to our previous work [25]. The contents of noble metal (Pt) and additive (Mo or Nb) were 2.0 wt% and 1.0 wt%, respectively.

2.2. Catalyst characterization

Powder X-ray diffraction (XRD) patterns were recorded with a Bruker D8 Advance diffractometer by using Cu K_α radiation, and the patterns were collected in the 2θ range from 10° to 90° with a scanning rate of 12° min^{-1}. Elemental Pt on the catalyst surface was analyzed by X-ray photoelectron spectroscopy (XPS) with a ThermoFischer ESCALAB 250Xi instrument with Al K_α (15 kV, 10.8 mA, $h\nu$ = 1486.6 eV) as the excitation light source under approximately 2 × 10^{-7} Pa ultrahigh vacuum, calibrated internally by the carbon deposit C (1*s*) (E_b = 284.6 eV). CO pulse adsorption for measurement of the CO chemical uptake and Pt dispersion was performed with a BELCAT II analyzer at 313 K. Before the measurement, the catalyst was reduced with a gas mixture (5% H_2 + 95% He, 30 mL min^{-1}) at 300 °C for 1 h and purged with He. TEM pictures of catalysts were obtained with a JEOL-2100F instrument. HAADF and EDS images were recorded on a Talos F200x instrument. Diffuse-reflectance infrared Fourier transform spectroscopy of CO chemisorption and in situ diffuse-reflectance infrared spectroscopy of alkane oxidation reactions were performed with a ThermoFischer Nicolet iS50 FTIR spectrometer according to our previous work [25].

2.3. Catalytic activity evaluation for short-chain alkane combustion

The catalytic combustion of short-chain alkanes was conducted in a fixed-bed quartz tubular reactor (*i.d.* = 6 mm) at atmospheric pressure. Catalysts (100 mg, 60–80 mesh) were diluted with quartz sand (100 mg) of the same size and put into the quartz tubular reactor. The gas mixtures were composed of 0.6% CH_4 + 2% O_2 + 97.4% N_2 or 0.3% C_2H_6 + 2% O_2 + 97.7% N_2 or 0.2% C_3H_8 + 2% O_2 + 97.8% N_2 with a total flow rate of

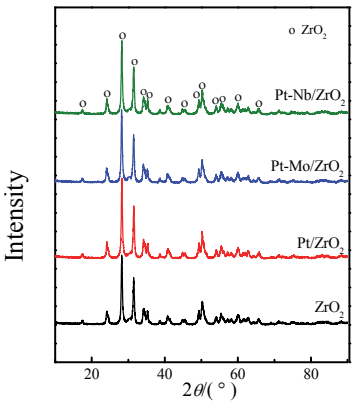

Fig. 1. XRD patterns of Pt/ZrO_2, $Pt\text{-}Mo/ZrO_2$, and $Pt\text{-}Nb/ZrO_2$ catalysts.

33.3 mL min^{-1} (mass space velocity (S.V.) of 20000 mL g^{-1} h^{-1}). Liquid *n*-hexane with saturated gas was put in a temperature-controlled saturator. An air flow (5 mL min^{-1}) passed through the saturator to give the desired partial pressure of *n*-hexane, which was diluted by another air flow with a speed of 300 mL min^{-1} before passing the catalyst bed. The mixture (0.2% *n*-hexane + 99.8% air) flow rate through the catalyst bed corresponded to a mass space velocity of 18300 mL g^{-1} h^{-1}. The concentrations of alkanes in the inlet ($[C]_{in}$) and outlet ($[C]_{out}$) gas could be detected with inline gas chromatography (Shimadzu GC-2014 instrument) equipped with a flame ionization detector and an HPGS-GASPRO capillary column (30 m × 0.32 mm). Conversion of the alkanes was calculated by using the following equation:

$$\text{Conversion} = ([C]_{in} - [C]_{out})/[C]_{in} \times 100\%.$$

It should be noted that no other by-products were detected (other than CO_2 and H_2O).

3. Results and discussion

3.1. General characterization of the catalysts

Fig. 1 shows the XRD patterns of the Pt/ZrO_2, $Pt\text{-}Mo/ZrO_2$, and $Pt\text{-}Nb/ZrO_2$ catalysts. All of the catalysts show the same characteristic diffraction peaks of the monoclinic ZrO_2 (PDF No. 78-0048) support. Characteristic peaks corresponding to MoO_x, NbO_x, and Pt/PtO_x are not observed in the catalysts, which indicates that both Pt species and promoters (Mo and Nb) are highly dispersed or amorphous.

Fig. 2 and Fig. S1 show the HAADF-STEM and HRTEM images and the particle size distributions of Pt species in the catalysts. The particles sizes of the Pt species are relatively uniform with mean diameters of approximately 2.0 nm for the Pt/ZrO_2, $Pt\text{-}Mo/ZrO_2$, and $Pt\text{-}Nb/ZrO_2$ catalysts. Thus, the addition of Mo and Nb has no influence on the mean particle size of the Pt species, which is consistent with our previous work [25].

Raman spectra of the catalysts are shown in Fig. 3. Bands at 192, 345, 391, 481, 569, and 643 cm^{-1} are observed for the Pt/ZrO_2 catalyst and are assigned to the ZrO_2 support, whereas these characteristic bands become significantly weaker after the introduction of Mo and Nb. The appearance of bands at 875 and 957 cm^{-1} indicates the presence of MoO_3 species in the $Pt\text{-}Mo/ZrO_2$ catalyst, and the weak band at 990 cm^{-1} is attributed to the Nb_2O_5 species in the $Pt\text{-}Nb/ZrO_2$ catalyst [25,27,28].

Surface acidity of the catalysts was measured by NH_3-TPD, and the profiles are shown in Fig. 4. Each catalyst exhibits NH_3 desorption peaks in the temperature ranges of 200–250 °C (peak α) and 400–500 °C (peak β), indicating the presence of medium acid sites and strong acid sites, respectively. It is interesting that Nb promotion results in an increase in medium acid sites, whereas Mo promotion results in additional strong

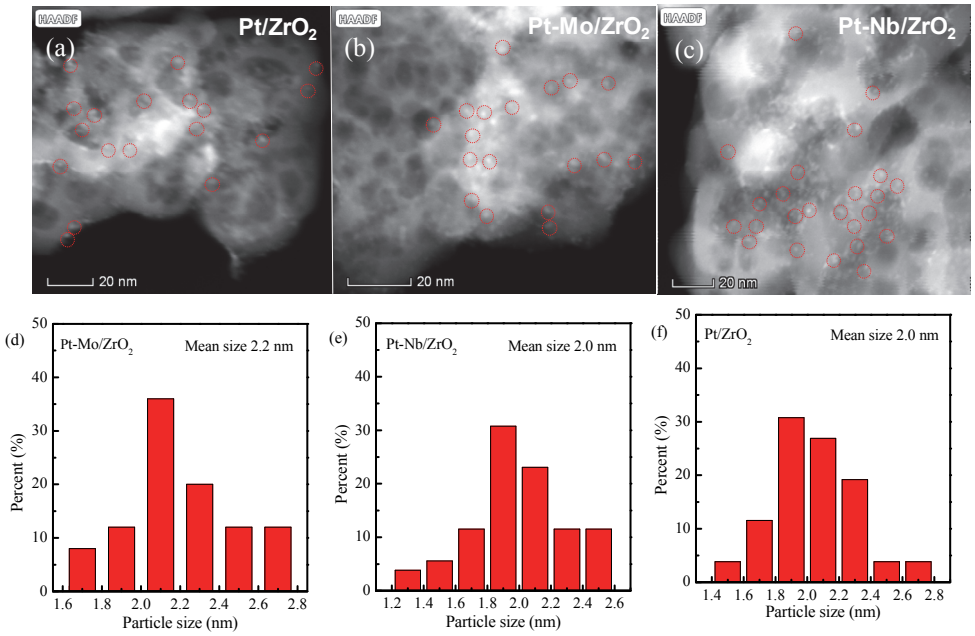

Fig. 2. TEM images (a–c) and particle size distributions (d–f) of Pt/ZrO_2 (a,d), $Pt\text{-}Mo/ZrO_2$ (b,e), and $Pt\text{-}Nb/ZrO_2$ (c,f) catalysts.

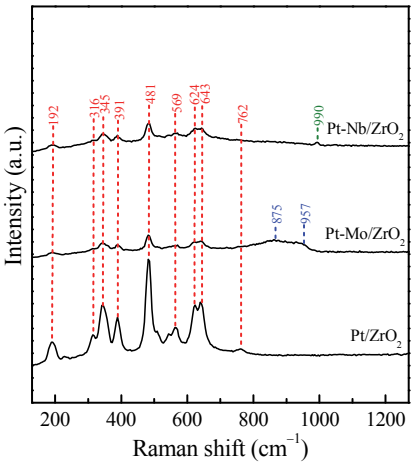

Fig. 3. Raman spectra of Pt/ZrO$_2$, Pt-Mo/ZrO$_2$, and Pt-Nb/ZrO$_2$ catalysts.

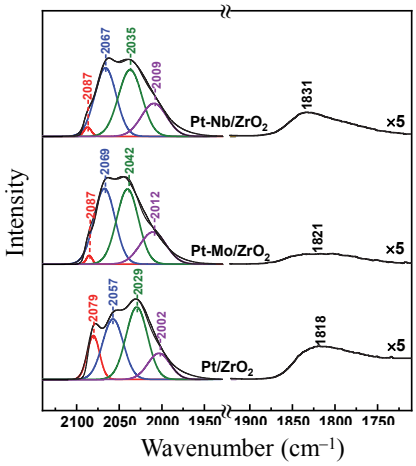

Fig. 5. DRIFT spectra of CO adsorption on Pt/ZrO$_2$, Pt-Mo/ZrO$_2$, and Pt-Nb/ZrO$_2$ catalysts at 25 °C.

acid sites.

Fig. 5 shows the *in situ* DRIFT spectra of CO adsorption on the catalysts at 25 °C. The Pt/ZrO$_2$ catalyst gives two bands at 1818 and 2000–2080 cm^{-1}, which could be assigned to bridged adsorption of CO on the adjacent Pt-Pt sites and linearly adsorbed CO on Pt atoms, respectively. Moreover, the latter band could be deconvoluted into four different bands at 2002, 2029, 2057, and 2079 cm^{-1}, corresponding to linearly adsorbed CO on different locations of Pt species [29]. The Pt-Mo/ZrO$_2$ and Pt-Nb/ZrO$_2$ catalysts give similar bands to Pt/ZrO$_2$. However, the bridged CO on the Pt-Mo/ZrO$_2$ catalyst has much less intensity than those on the Pt/ZrO$_2$ and Pt-Nb/ZrO$_2$ catalysts, indicating the coverage of Pt by MoO$_x$ species in Pt-Mo/ZrO$_2$. On the contrary, the addition of NbO$_x$ does not alter the surface structure of the Pt species and results in no obvious change of the bridged CO band.

3.2. Catalytic activity of methane and propane combustion

The catalytic activities of methane and propane combustion over the catalysts (Pt/ZrO$_2$, Pt-Mo/ZrO$_2$, and Pt-Nb/ZrO$_2$) and the supports (Mo/ZrO$_2$ and Nb/ZrO$_2$) are shown in Fig. 6. The supported Pt catalysts exhibit much higher activities than the pristine Mo/ZrO$_2$ and Nb/ZrO$_2$ supports, strongly suggesting that the Pt species are important active sites. Moreover, the temperature for complete methane oxidation is higher than that of propane over all catalysts, implying that methane is more difficult to oxidize. This can be ascribed to the fact that methane has higher C–H bond energy than propane (439.3 *vs.* 418.0 kJ·mol^{-1}) and a much more stable tetragonal structure. The activities of methane combustion over the catalysts decrease in the order: Pt-Nb/ZrO$_2$ > Pt/ZrO$_2$ > Pt-Mo/ZrO$_2$. However, the trend of propane combustion is significantly different from that of methane, namely, Pt-Mo/ZrO$_2$ > Pt-Nb/ZrO$_2$ > Pt/ZrO$_2$. Thus, it is clear that the addition of Mo in the Pt/ZrO$_2$ catalyst inhibits methane combustion but promotes propane combustion remarkably, whereas the addition of Nb promotes both methane and propane combustion but the Nb addition results in slightly lower enhancement than the Mo addition for propane combustion.

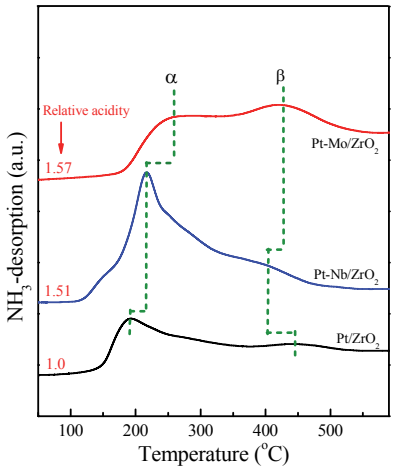

Fig. 4. NH$_3$-TPD profiles of Pt/ZrO$_2$, Pt-Mo/ZrO$_2$, and Pt-Nb/ZrO$_2$ catalysts.

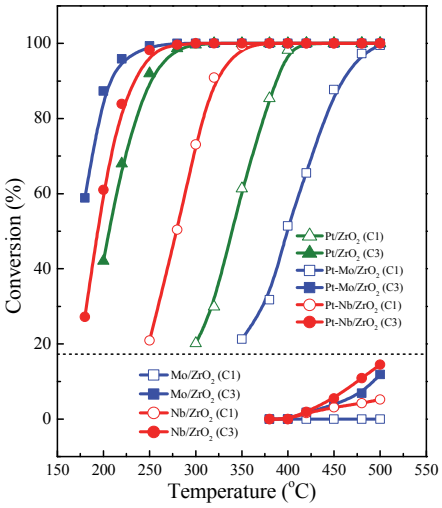

Fig. 6. Catalytic activity of methane and propane combustion over the Pt/ZrO$_2$, Pt-Mo/ZrO$_2$, and Pt-Nb/ZrO$_2$ catalysts and the Mo/ZrO$_2$ and Nb/ZrO$_2$ supports (C1 = methane, C3 = propane).

Table 1
CO chemisorption, specific reaction rates, and turnover frequencies (TOFs) of Pt/ZrO_2, $Pt\text{-}Mo/ZrO_2$, and $Pt\text{-}Nb/ZrO_2$ catalysts.

Catalyst	Pt content (wt.%)	Pt dispersion [a] (%)	CO uptake [a] (μmol g_{Pt}^{-1})	Specific reaction rate [b] (μmol g_{Pt}^{-1} s^{-1})		TOF ($\times10^{-3}$ s^{-1}) [c]	
				methane	propane	methane	propane
Pt/ZrO_2	2.1	30.0	30.7	45.9	15.9	29.4	10.2
$Pt\text{-}Mo/ZrO_2$	2.0	22.5	23.0	21.6	44.2	18.1	37.1
$Pt\text{-}Nb/ZrO_2$	2.0	31.4	32.2	96.6	19.0	57.4	11.3

[a] Pt dispersion and CO chemisorption were determined by CO pulse adsorption;
[b] based on methane conversion at 300 °C or propane conversion at 180 °C (the catalyst was decreased to a certain amount in order to calculate the TOF value under low conversion; details are summarized in Table S1);
[c] based on the CO chemisorption and methane conversion at 300 °C or propane conversion at 180 °C (the catalyst was decreased to a certain amount in order to calculate the TOF value under low conversion; details are summarized in Table S1).

Table 1 shows the Pt dispersion, CO chemisorption capacity, specific reaction rates, and TOF of the catalysts. The Pt dispersion is calculated according to the CO chemisorption result and decreases in the order: $Pt\text{-}Nb/ZrO_2$ (31.4%) > Pt/ZrO_2 (30.0%) > $Pt\text{-}Mo/ZrO_2$ (22.5%). The Pt dispersions of $Pt\text{-}Nb/ZrO_2$ and Pt/ZrO_2 are relatively close, and the Pt particle sizes calculated by CO chemisorption are 3.6 and 3.8 nm, respectively, whereas the HRTEM results reveal Pt particle sizes of approximately 2.0 nm for both catalysts. The Pt particle size calculated by CO chemisorption is slightly larger than that measured by HRTEM. This can be attributed to the fact that partial Pt particles enter the support pores and make contact with the support surface, thus decreasing the exposed surface Pt atoms [30]. However, the dispersion of Pt in $Pt\text{-}Mo/ZrO_2$ is only 22.5%, corresponding to a Pt particle size of 5.0 nm, which is significantly larger than those in the $Pt\text{-}Nb/ZrO_2$ and Pt/ZrO_2 catalysts as determined by CO chemisorption (3.6 and 3.8 nm, respectively) and is also larger than the particle size of 2.2 nm obtained by the HRTEM statistics method. These larger Pt particles in the $Pt\text{-}Mo/ZrO_2$ catalyst cannot be explained similarly to the cases of the Pt/ZrO_2 and $Pt\text{-}Nb/ZrO_2$ catalysts; instead, this result reflects the decoration effect of MoO_3 species on the Pt particle surface, whereas the Nb_2O_5 species on the support may be partially covered by Pt particles [25].

In order to compare the catalytic activity, the specific reaction rates and TOF values for methane and propane combustion over the catalysts were measured under kinetically controlled conditions and evaluated. For methane combustion, the Pt/ZrO_2 catalyst gives a specific reaction rate of 45.9 μmol g_{Pt}^{-1} s^{-1} and a TOF of 29.4×10^{-3} s^{-1} at 300 °C. The activity is significantly promoted over the $Pt\text{-}Nb/ZrO_2$ catalyst, which gives a specific reaction rate of 96.6 μmol g_{Pt}^{-1} s^{-1} and a TOF of 57.4×10^{-3} s^{-1}. However, the $Pt\text{-}Mo/ZrO_2$ catalyst gives a specific reaction rate of 21.6 μmol g_{Pt}^{-1} s^{-1} and a TOF of 18.1×10^{-3} s^{-1}, much lower values than those of Pt/ZrO_2. For propane combustion, the $Pt\text{-}Nb/ZrO_2$ catalyst gives similar activity to Pt/ZrO_2 (rates of 19.0 and 15.9 μmol g_{Pt}^{-1} s^{-1} and TOFs of 11.3 and 10.2×10^{-3} s^{-1}), whereas the $Pt\text{-}Mo/ZrO_2$ catalyst gives a much higher reaction rate (a specific rate of 44.2 μmol g_{Pt}^{-1} s^{-1} and a TOF of 37.1×10^{-3} s^{-1}). Therefore, it is clear that Nb and Mo play different roles in the combustion of methane and propane, which may be related to their different structural properties or surface chemistry.

Fig. 7 shows the stability tests for propane combustion over the Pt/ZrO_2, $Pt\text{-}Mo/ZrO_2$, and $Pt\text{-}Nb/ZrO_2$ catalysts. Considering the obvious activity differences of these catalysts for propane combustion, the catalytic stability tests were conducted at different temperatures (Pt/ZrO_2 at 250 °C with a conversion of 92%, $Pt\text{-}Mo/ZrO_2$ at 200 °C with a conversion of 87%, and $Pt\text{-}Nb/ZrO_2$ at 220 °C with a conversion of 84%) to control the propane conversion at 80%–90%. All of the catalysts are very stable during the reaction process.

3.3. Analysis of Pt species and acidity on catalyst surfaces

Fig. 8 shows the Pt 4*f* XPS spectra of the fresh and spent catalysts. The peaks with binding energies at 71.6 and 74.9 eV are assigned to Pt $4f_{7/2}$ and Pt $4f_{5/2}$ of the Pt^0 species, respectively. The signals at binding energies of 72.9 and 76.2 eV correspond to Pt $4f_{7/2}$ and Pt $4f_{5/2}$ of the Pt^{2+} species, respectively. The peaks of Pt $4f_{7/2}$ and Pt $4f_{5/2}$ related to the Pt^{4+} species appear at 74.6 and 77.9 eV, respectively. As summarized in Table 2, it is clear that the fresh catalysts contain mainly oxidized Pt species (i.e., Pt^{2+} and Pt^{4+}). In the spent catalysts (used for either methane or propane combustion), the content of metallic Pt^0 species increases, implying the reduction of Pt oxides by alkane molecules during the reaction.

3.4. Brief discussion on different roles of the promoters in the

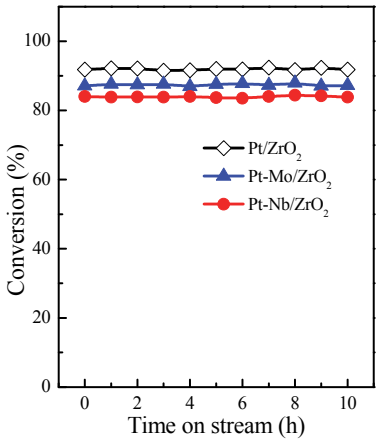

Fig. 7. Stability tests of Pt/ZrO_2, $Pt\text{-}Mo/ZrO_2$, and $Pt\text{-}Nb/ZrO_2$ catalysts at different temperatures for propane (0.2% C_3H_8 + 2% O_2 + 97.8% N_2, S.V. = 20000 h^{-1}).

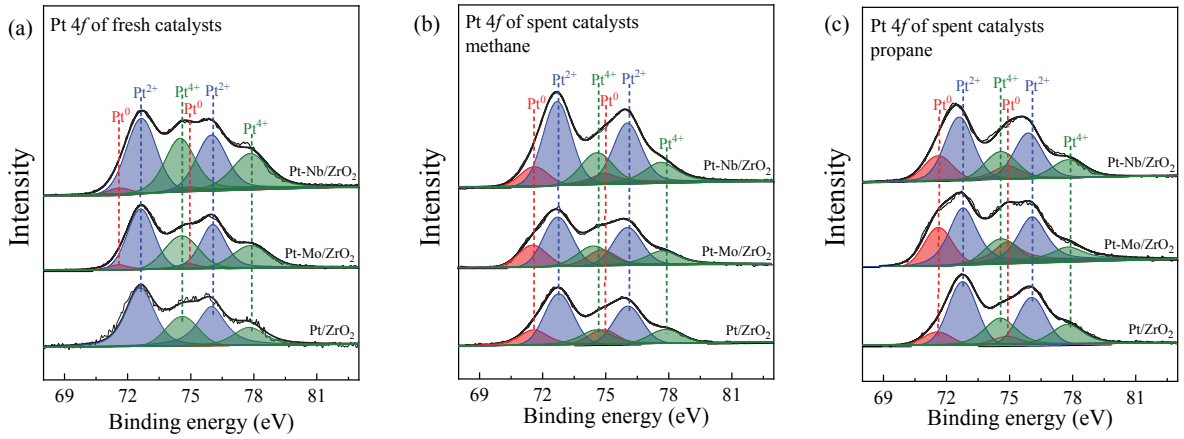

Fig. 8. Pt 4*f* XPS spectra of Pt/ZrO_2, $Pt\text{-}Mo/ZrO_2$, and $Pt\text{-}Nb/ZrO_2$ catalysts.

reactions

Interestingly, the promotion of NbO_x and MoO_x in the Pt/ZrO_2 catalysts results in very different reaction behaviors in methane and propane combustion, which is related to the different structures and surface properties of the catalysts, as well as the different active sites required for the reactions. First, although the promotion of NbO_x and MoO_x in Pt/ZrO_2 does not alter the Pt particle sizes in the catalysts (Fig. 2), the promoter-Pt interactions are changed, particularly with regard to the formation of promoter-Pt interfaces. The CO uptake results clearly suggest the formation of more accessible MoO_x-Pt interfacial sites on the $Pt\text{-}Mo/ZrO_2$ catalyst surface, whereas there are negligible accessible $Pt\text{-}NbO_x$ interfacial sites on the $Pt\text{-}Nb/ZrO_2$ catalyst surface. It is well recognized that, for Pt catalysts, the $Pt\text{-}MO_x$ interfacial sites are very active for propane combustion, as a result of the facile activation of propane molecules on the interfacial sites. For example, Liao *et al.* [24] reported that a WO_3-promoted Pt/BN catalyst was much more active than bare Pt/BN for propane combustion because propane could be easily activated on the hydroxyl groups in the WO_3 and reacts with oxygen species adsorbed on adjacent Pt species; thus, the activity was significantly improved. Moreover, Zhao *et al.* [25] concluded that the $Pt\text{-}MoO_3$ interfacial site in the $Pt\text{-}MoO_3/ZrO_2$ catalyst gave forty-fold higher activity than the surface Pt sites. Therefore, the formation of $Pt\text{-}MoO_3$ in the current work is certainly beneficial for the enhancement of reactivity. In this sense, the lack of enough accessible $Pt\text{-}NbO_x$ interfacial sites in the $Pt\text{-}Nb/ZrO_2$ catalyst may not be helpful for the promotion of activity. On the other hand, the decoration of Pt nanoparticles by MoO_x leads to fewer exposed surface Pt atoms, which thus greatly inhibits the activity for methane combustion because it has been claimed that surface Pt atoms are the active sites for this reaction [31].

In addition, the Mo and Nb promotion of the Pt/ZrO_2 catalysts also changes the oxidation states of the Pt species, which is a crucial parameter for alkane combustion. It has been well recognized that oxidized Pt species are favorable for methane combustion [19], whereas metallic Pt species are favorable for propane combustion [23,32–34]. In the current study, the $Pt\text{-}Nb/ZrO_2$ catalyst gives the highest Pt^{n+} surface concentration (86.6, Table 2) after the methane combustion reaction, in comparison with those of the Pt/ZrO_2 and $Pt\text{-}Mo/ZrO_2$ catalysts, which suggests that the addition of NbO_x can somehow stabilize the Pt species in high oxidation states and thus enhance activity for methane combustion. In contrast, the $Pt\text{-}Mo/ZrO_2$ catalyst gives a relatively higher concentration of Pt^0 species (and lower concentration of Pt^{n+} species) because of the reduction of platinum oxide by methane, which explains its lower activity for methane combustion. Moreover, Mo and Nb promotion leads to increased surface acidity (Fig. 8), which is beneficial for the adsorption and activation of longer chain alkanes such as propane, but the direct activation and adsorption of methane is very difficult [35,36]. Also, Zhao *et al.* [25] reported that an increased number of acid sites (especially strong acid sites) is favorable for the generation of Pt^0 species, which are important active sites for propane combustion.

The structural and surface properties upon Mo and Nb promotion of the Pt/ZrO_2 catalyst and their different roles in methane and propane combustion are illustrated in Scheme 1.

Table 2
Analysis of Pt species content on fresh and spent catalyst surfaces.

Catalyst	Fresh catalyst (%)			After methane combustion [a] (%)			After propane combustion [b] (%)		
	Pt^0	Pt^{2+}	Pt^{4+}	Pt^0	Pt^{2+}	Pt^{4+}	Pt^0	Pt^{2+}	Pt^{4+}
Pt/ZrO_2	0	62.0	38.0	20.5	56.7	22.8	11.9	56.0	32.1
$Pt\text{-}Mo/ZrO_2$	6.2	56.6	37.2	23.6	54.3	22.1	28.9	51.8	19.3
$Pt\text{-}Nb/ZrO_2$	4.2	53.7	42.1	13.4	61.3	25.3	20.1	54.8	25.1

[a] spent catalysts after methane combustion reaction;
[b] spent catalysts after propane combustion reaction.

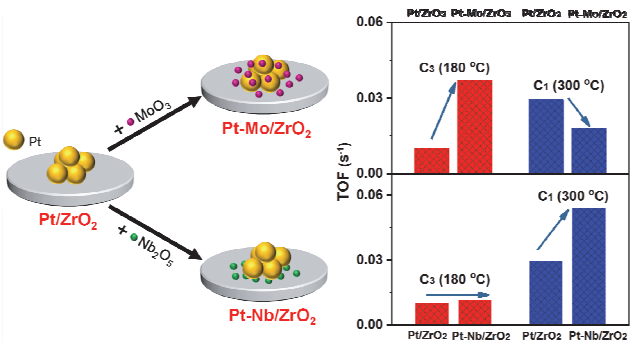

Scheme 1. Structure models for propane and methane combustion over Pt/ZrO_2, $Pt\text{-}Mo/ZrO_2$, and $Pt\text{-}Nb/ZrO_2$ catalysts.

The addition of MoO_3 in the catalyst generates $Pt\text{-}MoO_3$ interfaces and enhances the surface acidity, which leads to the improved activity for propane combustion; however, such $Pt\text{-}MoO_3$ interfaces are not favorable for methane combustion because the reaction requires exposed surface Pt atoms rather than $Pt\text{-}MoO_3$ interfacial sites. The addition of Nb_2O_5 in the catalyst does not generate enough accessible $Pt\text{-}Nb_2O_5$ interfacial sites on the $Pt\text{-}Nb/ZrO_2$ catalyst surface; thus, the slight improvement in the propane combustion is attributed to the enhanced surface acidity. On the other hand, cationic Pt^{n+} species can be stabilized by the addition of Nb_2O_5 under the methane combustion atmosphere, which accounts for the significant improvement in the activity for methane combustion.

To clearly reveal the catalytic activity trend with other short-chain alkanes over the Pt/ZrO_2, $Pt\text{-}Mo/ZrO_2$, and $Pt\text{-}Nb/ZrO_2$ catalysts, the catalytic combustion reactions of ethane and *n*-hexane were also investigated (Fig. 9). With respect to the oxidation of ethane, the $Pt\text{-}Nb/ZrO_2$ and Pt/ZrO_2 catalysts showed similar activity trends to those of the methane reaction, namely, $Pt\text{-}Nb/ZrO_2$ > Pt/ZrO_2. However, the catalytic activity of ethane oxidation over the $Pt\text{-}Mo/ZrO_2$ catalyst was obviously improved relative to that with the Pt/ZrO_2 catalyst (methane activity: Pt/ZrO_2 > $Pt\text{-}Mo/ZrO_2$; ethane activity: $Pt\text{-}Mo/ZrO_2$ > Pt/ZrO_2), which might be a result of the existence of the C–C bond (377.4 kJ·mol^{-1}) in ethane. In addition, the $Pt\text{-}Mo/ZrO_2$ catalyst showed the highest catalytic activity for both propane and *n*-hexane, which confirms that the $Pt\text{-}Mo/ZrO_2$ catalyst is more favorable for the activation of C–C bonds and acceleration of the combustion reaction of alkanes containing C–C bonds, whereas the $Pt\text{-}Nb/ZrO_2$ catalyst is more beneficial for the activation of high-energy C–H bonds (methane activity: $Pt\text{-}Nb/ZrO_2$ > Pt/ZrO_2 > $Pt\text{-}Mo/ZrO_2$; ethane activity: $Pt\text{-}Nb/ZrO_2$ > $Pt\text{-}Mo/ZrO_2$ > Pt/ZrO_2; propane activity: $Pt\text{-}Mo/ZrO_2$ > $Pt\text{-}Nb/ZrO_2$ > Pt/ZrO_2; *n*-hexane activity: $Pt\text{-}Mo/ZrO_2$ > $Pt\text{-}Nb/ZrO_2$ > Pt/ZrO_2). Moreover, it can be observed that the inhibition of MoO_3 (for methane) dramatically transforms into promotion (for ethane, propane, and *n*-hexane) with the increase of the carbon chain length, but the remarkable promotion of Nb_2O_5 is gradually weakened as the carbon chain length increases from methane to *n*-hexane. In the *in situ* DRIFT spectra of alkane oxidation (methane, ethane, and propane) over the catalysts (Figs. S2–S4), the vibration peak at 2012–2128 cm^{-1} ascribed to intermediate CO adsorbed on Pt species is obviously more noticeable for $Pt\text{-}Mo/ZrO_2$ and $Pt\text{-}Nb/ZrO_2$ than for Pt/ZrO_2, implying that the promotion of MoO_3 and Nb_2O_5 indeed changes the reaction path and mechanism of alkane combustion over the Pt/ZrO_2 catalyst.

4. Conclusions

In summary, this study reveals that Mo and Nb promotion shows obviously different effects on the catalytic combustion of short-chain alkanes (methane, ethane, propane, and *n*-hexane) over Pt/ZrO_2 catalysts. The MoO_3 promoter inhibits the combustion of methane but promotes the combustion of ethane, propane, and *n*-hexane. The promotion of Nb_2O_5 weakens as the carbon chain length of the alkane increases. A detailed study of the methane and propane oxidation reactions over the catalysts reveals that such differences lie in the different structural properties of the catalysts and the chemical states of the Pt species. The generation of $Pt\text{-}MoO_x$ interfaces, a high concentration of metallic Pt surface species, and an enhanced surface acidity are the main reasons for the improved activity for propane combustion over the $Pt\text{-}Mo/ZrO_2$ catalyst, but these facts are not favorable for the methane combustion because it requires oxidized surface Pt species. The addition of Nb_2O_5 to Pt/ZrO_2 does not generate accessible $Pt\text{-}Nb_2O_5$ interface sites on the catalyst surface but stabilizes Pt^{n+} species under the

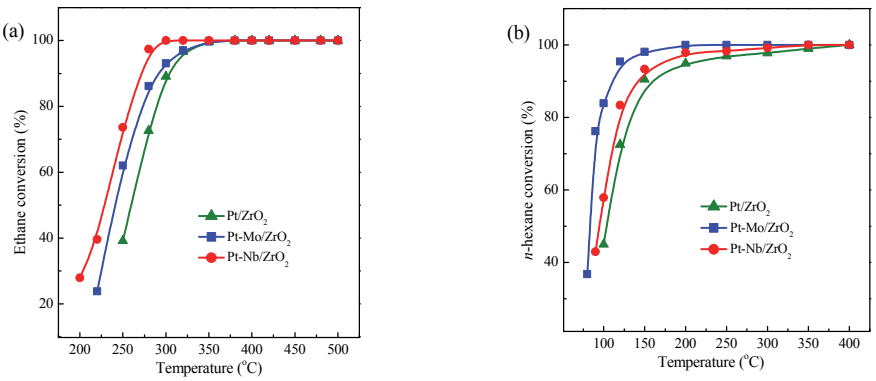

Fig. 9. Relationship between ethane (a) and *n*-hexane (b) conversion rates and reaction temperatures for Pt/ZrO_2, $Pt\text{-}Mo/ZrO_2$, and $Pt\text{-}Nb/ZrO_2$ catalysts.

Graphical Abstract

Chin. J. Catal., 2021, 42: 2287–2295 doi: 10.1016/S1872-2067(20)63771-8

Different roles of MoO_3 and Nb_2O_5 promotion in short-chain alkane combustion over Pt/ZrO_2 catalysts

Bingheng Cen, Cen Tang, Jiqing Lu, Jian Chen *, Mengfei Luo *
Zhejiang Normal University

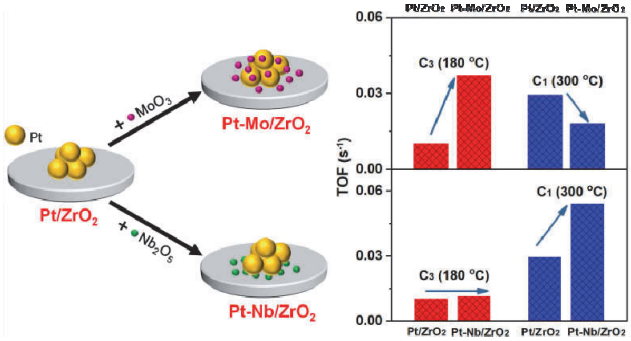

Different roles of MoO_3 and Nb_2O_5 promotion in short-chain alkane combustion over Pt/ZrO_2 catalysts are revealed. MoO_3 is favorable for the activation of C–C bonds, whereas Nb_2O_5 is more beneficial for the activation of C–H bonds.

methane combustion atmosphere and thus enhances the activity for methane combustion. MoO_3 promotion is more favorable for the activation of C–C bonds and acceleration of the combustion of alkanes containing C–C bonds, but Nb_2O_5 promotion is more beneficial for the activation of high-energy C–H bonds.

Electronic supporting information

Supporting information is available in the online version of this article.

References

[1] C. He, J. Cheng, X. Zhang, M. Douthwaite, S. Pattisson, Z. Hao, *Chem. Rev.*, **2019**, 119, 4471–4568.
[2] M. S. Kamal, S. Razzak, M. M. Hossain, *Atmos. Environ.*, **2016**, 140,117–134.
[3] L. Zhang, W. Deng, Y. Cai, Q. Dai, L. Guo, *ACS Catal.*, **2020**, 10, 13109–13124.
[4] A. Zhu, Y. Zhou, Y. Wang, Q. Zhu, H. Liu, Z. Zhang, H. Lu, *J. Rare Earths*, **2018**, 36, 1272–1277.
[5] B. Zhou, X. Zhang, Y. Wang, J. Xie, K. Xi, Y. Zhou, H. Lu, *J. Environ. Sci.*, **2019**, 84, 59–68.
[6] W. Deng, Q. Tang, S. Huang, L. Zhang, Z. Jia, L. Guo, *Appl. Catal. B*, **2020**, 278, 119336.
[7] Y. Wang, L. Guo, M. Chen, C. Shi, *Catal. Sci. Technol.*, **2018**, 8, 459–471.
[8] P. Losch, W. Huang, O. Vozniuk, E. D. Goodman, W. Schmidt, M. Cargnello, *ACS Catal.*, **2019**, 9, 4742–4753.
[9] T. Kondratowicz, M. Drozdek, M. Michalik, W. Gac, M. Gajewska, P. Kuśtrowski, *Appl. Surf. Sci.*, **2020**, 513, 145788.
[10] Z. Fei, P. Lu, X. Feng, B. Sun, W. Ji, *Catal. Sci. Technol.*, **2012**, 2, 1705–1710.
[11] W. Hu, Z. Shao, X. Cao, P. Hu, *Chin. J. Catal.*, **2020**, 41, 1369–1377.
[12] Z. Feng, Q. Ren, R. Peng, S. Mo, M. Zhang, M. Fu, L. Chen, D. Ye, *Catal. Today*, **2019**, 332, 177–182.
[13] K. Murata, J. Ohyama, Y. Yamamoto, S. Arai, A. Satsuma, *ACS Catal.*, **2020**, 10, 8149–8156.
[14] E. D. Goodman, S. Dai, A. C. Yang, C. J. Wrasman, A. Gallo, S. R. Bare, A. S. Hoffman, T. F. Jaramillo, G. W. Graham, X. Pan, M. Cargnello, *ACS Catal.*, **2017**, 7, 4372–4380.
[15] W. Huang, X. Zhang, A. C. Yang, E. D. Goodman, K. C. Kao, M. Cargnello, *ACS Catal.*, **2020**, 10, 8157–8167.
[16] R. Li, L. Zhang, S. Zhu, S. Fu, X. Dong, S. Ida, L. Zhang, L. Guo, *Appl. Catal. A*, **2020**, 602, 117715.
[17] B. Zhao, Y. Jian, Z. Jiang, R. Albilali, C. He, *Chin. J. Catal.*, **2019**, 40, 543–552.
[18] Z. Zhu, G. Lu, Z. Zhang, Y. Guo, Y. Guo, Y. Wang, *ACS Catal.*, **2013**, 3, 1154–1164.
[19] J. Yang, M. Peng, G. Ren, H. Qi, X. Zhou, J. Xu, F. Deng, Z. Chen, J. Zhang, K. Liu, X. Pan, W. Liu, Y. Su, W. Li, B. Qiao, D. Ma, T. Zhang, *Angew. Chem. Int. Ed.*, **2020**, 59, 18522–18526.
[20] J. Chen, J. Zhong, Y. Wu, W. Hu, P. Qu, X. Xiao, G. Zhang, X. Liu, Y. Jiao, L. Zhong, Y. Chen, *ACS Catal.*, **2020**, 10, 10339–10349.
[21] P. Zhao, X. Li, W. Liao, Y. Wang, J. Chen, J. Lu, M. Luo, *Ind. Eng. Chem. Res.*, **2019**, 58, 21945–21952.
[22] W. Tang, Z. P. Hu, M. Wang, G. D. Stucky, H. Metiu, E. W. McFarland, *J. Catal.*, **2010**, 273, 125–137.
[23] Y. Liu, X. Li, W. M. Liao, A. P. Jia, Y. J. Wang, M. F. Luo, J. Q. Lu, *ACS Catal.*, **2019**, 9, 1472–1481.
[24] W. M. Liao, X. X. Fang, B. H. Cen, J. Chen, Y. R. Liu, M. F. Luo, J. Q. Lu, *Appl. Catal. B*, **2020**, 272, 118858.
[25] P. P. Zhao, J. Chen, H. B. Yu, B. H. Cen, W. Y. Wang, M. F. Luo, J. Q. Lu, *J. Catal.*, **2020**, 391, 80–90.
[26] H. Hao, B. Jin, W. Liu, X. Wu, F. Yin, S. Liu, *ACS Catal.*, **2020**, 10, 13543–13548.
[27] J. Jia, P. G. O'Brien, L. He, Q. Qiao, T. Fei, L. M. Reyes, T. E. Burrow, Y. Dong, K. Liao, M. Varela, S. J. Pennycook, M. Hmadeh, A. S. Helmy, N. P. Kherani, D. D. Perovic, G. A. Ozin, *Adv. Sci.*, **2016**, 3, 1600189.
[28] M. P. F. Graça, A. Meireles, C. Nico, M. A. Valente, *J. Alloys Compd.*, **2013**, 553, 177–182.
[29] S. Rimaz, L. Chen, A. Monzón; S. Kawi; A. Borgna, *Chem. Eng. J.*, **2021**, 405, 126656.
[30] G. Lan, H. Tang, Y. Zhou, W. Han, H. Liu, X. Li, Y. Li, *ChemCatChem*, **2014**, 6, 353–360.
[31] I. E. Beck, V. I. Bukhtiyarov, I. Yu. Pakharukov, V. I. Zaikovsky, V. V. Kriventsov, V. N. Parmon, *J. Catal.*, **2009**, 268, 60–67.
[32] H. Yoshida, Y. Yazawa, T. Hattori, *Catal. Today*, **2003**, 87, 19–28.
[33] Y. Yazawa, H. Yoshida, T. Hattori, *Appl. Catal. A*, **2002**, 237, 139–148.

[34] Y. Yazawa, N. Takagi, H. Yoshida, S. Komai, A. Satsuma, T. Tanaka, S. Yoshida, T. Hattori, *Appl. Catal. A*, **2002**, 233, 103–112.
[35] N. Kaylor, R. J. Davis, *J. Catal.*, **2018**, 367, 181–193.
[36] Q. Dai, Q. Zhu, Y. Lou, X. Wang, *J. Catal.*, **2018**, 357, 29–40.

MoO_3和Nb_2O_5助剂对Pt/ZrO_2催化剂上短链烷烃燃烧反应的不同促进作用

岑丙横, 汤 岑, 鲁继青, 陈 建#, 罗孟飞*
浙江师范大学物理化学研究所, 先进催化材料教育部重点实验室, 浙江省固体表面反应化学重点实验室, 浙江金华321004

摘要: 贵金属Pt催化剂具有高活性和热稳定性, 广泛应用于催化挥发性有机物的完全氧化反应(燃烧反应). 短链烷烃(甲烷、乙烷、丙烷等)化学性质稳定, 是最难氧化的一类有机物, 常用作考察燃烧反应催化剂性能的模型反应物. 然而, 目前报道的研究工作通常仅限于针对某一种烷烃底物的催化燃烧, 系统考察催化剂以及助剂对不同短链烷烃的催化燃烧活性鲜有报道. 在短链烷烃中, 甲烷只有C–H键; 而其它烷烃除了C–H键; 还有C–C键. 因此, 研究催化剂对甲烷、乙烷和丙烷燃烧反应催化性能的差异性, 对于认识催化剂上C–H键和C–C键的活化具有非常重要的意义.

本文制备了MoO_3或Nb_2O_5修饰的Pt/ZrO_2催化剂并用于短链烷烃的燃烧反应. 研究发现, MoO_3助剂对甲烷燃烧有明显的抑制作用, 但对乙烷, 丙烷和正己烷燃烧反应具有促进作用, 促进作用随着烷烃碳链的增长逐渐增加; Nb_2O_5助剂对甲烷、乙烷、丙烷和正己烷燃烧反应均具有促进作用, 然而促进作用随着碳链的增长而逐渐减弱. MoO_3和Nb_2O_5助剂的不同促进作用与助剂影响催化剂表面酸性以及Pt物种的氧化或还原态有关. NH_3-TPD结果表明, MoO_3助剂可以显著增加Pt/ZrO_2催化剂表面强酸位点数量, 而Nb_2O_5助剂可以显著增加Pt/ZrO_2催化剂表面中强酸位点数量. HTEM结果表明, 两种助剂的添加都不会明显改变Pt物种的颗粒尺寸. 在$Pt\text{-}Mo/ZrO_2$催化剂上, MoO_3覆盖部分Pt物种形成丰富的$Pt\text{-}MoO_3$界面, 促进了金属Pt物种和强表面酸性位点的生成, 提高了丙烷燃烧反应活性; $Pt\text{-}Nb/ZrO_2$催化剂上载体表面的部分Nb_2O_5被Pt物种包覆, 使得生成的表面$Pt\text{-}Nb_2O_5$界面低于$Pt\text{-}Mo/ZrO_2$催化剂, 但由于催化剂表面酸性位的提升, 也促进了丙烷燃烧反应活性的提高. XPS结果表明, 在甲烷燃烧反应中, $Pt\text{-}Nb/ZrO_2$催化剂上Pt^{n+}物种能够更加稳定地存在, 这可能是Nb_2O_5助剂提高$Pt\text{-}Nb/ZrO_2$催化剂上甲烷燃烧活性的关键. 而$Pt\text{-}Mo/ZrO_2$催化剂上Pt^{n+}物种在甲烷反应中可以更容易地被还原, 并且由于MoO_3的包裹导致暴露的Pt位点数量降低, 使催化剂催化甲烷燃烧的活性受到抑制. 可见, MoO_3助剂更有利于C–C键活化, 而Nb_2O_5助剂更有利于高键能的C–H键活化.

综上, 本文系统性地研究MoO_3助剂和Nb_2O_5助剂对Pt/ZrO_2催化剂上不同短链烷烃的燃烧反应的影响, 证实了两种助剂的促进作用与碳链长度的关系是截然不同的.

关键词: Pt/ZrO_2催化剂; 烷烃燃烧; MoO_3助剂; Nb_2O_5助剂; 活性位点

收稿日期: 2020-12-23. 接受日期: 2021-01-28. 上网时间: 2021-09-10.
*通讯联系人. 电子信箱: mengfeiluo@zjnu.cn
#通讯联系人. 电子信箱: jianchen@zjnu.cn
基金来源: 国家自然科学基金面上项目(21872124, 22072137).
本文的电子版全文由Elsevier出版社在ScienceDirect上出版(http://www.sciencedirect.com/journal/chinese-journal-of-catalysis).